CHIN. PHYS. LETT. Vol. 33, No. 3 (2016) 036101

Bubble Generation in Germanate Glass Induced by Femtosecond Laser *

Jue-Chen Wang(王珏晨)[1], Qiang-Bing Guo(郭强兵)[1], Xiao-Feng Liu(刘小峰)[1], Ye Dai(戴晔)[3], Zhi-Yu Wang(王智宇)[1], Jian-Rong Qiu(邱建荣)[1,2]**

[1]*School of Materials Science and Engineering, Zhejiang University, Hangzhou 310027*
[2]*State Key Laboratory of Luminescent Materials and Devices, South China University of Technology, Guangzhou 510640*
[3]*Department of Physics, Shanghai University, Shanghai 200444*

(Received 9 November 2015)

We report the observation of bubble generation and migration in a germanate glass during irradiation by a femtosecond laser of high repetition rate. Bubbles are formed around the focal area of the laser beam, and their movement indicates the presence of thermal gravity convection in the glass melt, which is beyond the existing theoretical model about temperature field of focal area. Inside the bubbles, oxygen molecules are observed by the confocal Raman micro-spectroscopy. The generation of molecular oxygen and bubbles is explained in terms of the spatial separation of Ge and O ions and micro-explosion inside the glass melt.

PACS: 61.43.Fs, 61.72.Qq, 52.38.Mf, 42.65.Re, 78.30.−j DOI: 10.1088/0256-307X/33/3/036101

Modification of transparent materials with ultrashort pulsed lasers has been extensively studied in recent decades due to its unique advantages in three-dimensional processing of materials. When a low repetition rate ultrafast laser beam is tightly focused inside the bulk of a transparent solid, usually a void-like structure could be produced in pristine materials via confined micro-explosion[1,2] and the accompanied spatial separation of elements in the plasma.[3,4] These micrometer scale structures are however too small for some optical applications. In comparison, the high repetition rate (multiple pulses) ultrafast laser has the advantage of high accuracy, small collateral damage, and large surface modification rate within a short period of time, which enables wide applications in the fabrication of waveguides, three-dimensional (3D) micro fluidic devices and data storage devices.[5−11] Therefore, the high repetition rate ultrafast laser microprocessing through separation of spatial elements will be amenable to the modification of more sophisticated controllable structures.

Usually, an ultrafast laser can generate bubbles in fluid systems, and this process can be utilized for the manipulation of carbon nanotubes, and the generation of the shock wave.[12,13] Similarly, in transparent solid materials such as glass, the ultrafast laser generates a micrometer-scale liquid region and leads to the formation of bubbles, which may have potential applications in optical devices such as bubble switches.[14] Previous research has shown the presence of various voids or bubbles in the focal area of ultrafast lasers.[2,15−18] The void structures induced by a single pulse have been widely investigated. However, the origin of the bubbles induced by the high repetition femtosecond laser remains unclear.[19]

In this Letter, we report bubble generation in germanate glasses induced by a femtosecond laser with the repetition rate of 250 kHz.[16,19] Thermodynamic effects of the bubble such as nucleation, coalescence and hydrodynamic effects are also discussed. Furthermore, inside each void, molecular oxygen was observed by Raman spectra inside the bubble structures due to spatial separation of Ge and O ions in the glass. Unlike the bubbles induced in borosilicate glass,[19] thermal convection of the germanate glass melt around the focal area is observed, where viscous forces in the melt also play an important role in triggering the motion of bubbles in glass melt.[20]

A glass with the composition of $85GeO_2$-$15Na_2O$ (mol.%) was prepared for the present study by a standard melt-quenching technique. Reagent grade GeO_2 and Na_2CO_3 were used as the raw materials. A batch of 20 g mixture was well grounded and melted in a platinum crucible at 1410℃ for 1 h in air. The melt was then cast onto a cold steel plate and quickly quenched with another plate. Thus a transparent and colorless glass sample was obtained. After annealing at 500℃ for 10 h, the samples were cut and polished into dimensions of 10 mm × 10 mm × 2 mm for further experiment.

A regenerative amplified 800 nm Ti:sapphire laser (RegA 9000, Coherent, Inc.) with 120 fs, 250 kHz mode-locked pulse was employed as the laser source in the experiment. The laser beam was tightly fo-

*Supported by the National Natural Science Foundation of China under Grant Nos 51132004 and 61475047, the National Basic Research Program of China under Grant No 2011CB808100, the Natural Science Foundation of Guangdong Province under Grant No S2011030001349, the Fundamental Research Funds for the Central Universities under Grant No 2013ZM0001, and the Open Fund of the State Key Laboratory of High Field Laser Physics of Shanghai Institute of Optics and Fine Mechanics.

**Corresponding author. Email: qjr@zju.edu.cn

© 2016 Chinese Physical Society and IOP Publishing Ltd

cused beneath the surface of the glass sample translated by an XYZ stage via a 50× microscope objective (NA=0.8). The pulse energy and irradiation time were tuned by a neutral density filter and a mechanical shutter, respectively. After the femtosecond laser irradiation, the induced structure of the glass sample was characterized with a confocal Raman spectroscopy system (Renishaw inVia) by using a 514 nm Ar^+ laser as the excitation sources. The optical microscope image around the laser focal area was taken by using the same micro-Raman system.

The optical images of the modified structures induced by static femtosecond laser pulses under different laser focal depths, irradiation time and laser powers are shown in Fig. 1. Here the focal depth is defined as the depth of the focal spot beneath the sample surface. Spherical structures are observed in the focal region of the laser beam, and the circular boundaries indicate a well-defined refractive index variation.

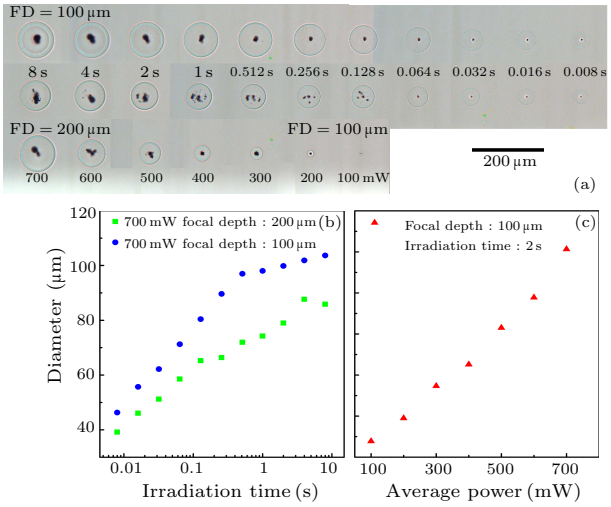

Fig. 1. (a) Optical microscope images of the femtosecond-laser-irradiated areas (1st line: laser power 700 mW, irradiation time 1/125–8 s, laser focal depth (FD) 100 μm; 2nd line: laser power 700 mW, irradiation time 1/125–8 s, laser focal depth 200 μm; 3rd line: laser power 100–700 mW, irradiation time 2 s, laser focal depth 100 μm). The dependences of diameters of dots on the irradiation time (b) and on the average laser power (c).

The formation of the inner boundary has been attributed to the generation of the thermal stress wave after photon excitation,[21] while the formation of outermost boundary may result from the stress between non-relaxed and relaxed materials due to a viscoelastic deformation mechanism.[22] No extra circular structures are found except for the two distinct ring-shaped boundaries, which differ from the appearance of a femtosecond modified region in previous reports.[22–25] This may suggest the difference in the temperature distribution in the irradiated area.[22] The single black dots inside the inner boundary of the spherical modified structure are bubbles with different shapes and sizes, which can be easily recognized in Figs. 1 and 2.

Furthermore, the diameter of the laser-induced spherical structures grows rapidly with the increase of the irradiation time. When the laser irradiation time is fixed, a linear relationship is observed between the diameter of the modified region and the average laser power. The slope change in Fig. 1(b) indicates that the expansion of the modified region may be dominated by different inherent mechanisms.[22] Under irradiation with the laser power of 700 mW and the focal depth of 100 μm, the outer boundary of the modified structure can be hardly seen for the irradiation time from 1/125 to 1/2 s, while it appears as the irradiation time increases. This phenomenon is also observed with the focal depth of 200 μm after irradiation for 4 s. We can assume that the expansion of the round structures mainly stems from the inner region under the short exposure time. After irradiation for a certain duration, the glass melt in the inner boundary begins to establish a dynamic equilibrium between the deposited energy from the incident laser and the diffusion energy to the surrounding areas.[10] Meanwhile, the viscoelastic deformation in the area between the inner and outer boundary leads to the further expansion of the round structures with the increase of the irradiation time.[22]

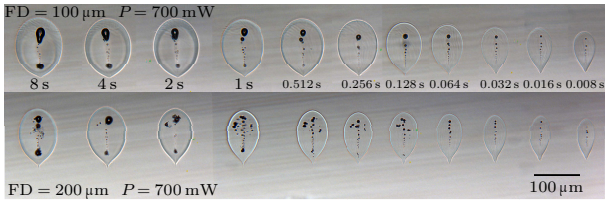

Fig. 2. Cross section of the femtosecond laser irradiated areas under optical transmission view (1st line: laser power 700 mW, irradiation time 1/125–8 s, laser focal depth 100 μm; 2nd line: laser power 700 mW, irradiation time 1/125–8 s, laser focal depth 200 μm).

The side view of the modified structures is shown in Fig. 2. The elliptic boundaries also indicate the refractive index variation of the modified area correspond to these in Fig. 1. The large bubbles are located at the top center of each modified structure, followed by an array of small bubbles. The small bubbles are around several micrometers in size, and their sizes increase as they approach the larger ones located at the top. More importantly, the number of small bubbles is reduced with the increase of the irradiation time. These facts suggest that the large bubbles are formed by the merging of small bubbles during continuous laser irradiation. Moreover, the line of bubbles appears turbulent with the increase of the irradiation duration, especially under the focal depth of 200 μm. Currently, reporting is rare on such bubble kinematics in the focal area of the femtosecond laser.

On the other hand, in the present case of laser irradiation at 250 kHz into a single spot, the photoexcita-

tion by the following pulses occurs before the heat generated by the previous pulses diffuses out of the photoexcited region. This is due to the fact that the time interval (∼4 μs) between successive pulses is less than the thermal diffusion time (∼10 μs).[22] As a result, the temperature of the solid glass around the focal area would increase due to the accumulated heat, leading to the melting of glass.[22,26] The temperature rise finally leads to the expansion of the melt volume with irradiation time, which can be clearly observed from the growth in size of the laser affected area (Fig. 2).

Concerning the physicochemical process for the formation of laser-induced microstructure in glass, previous research on optical discharge in fiber showed that the cavern structure could be induced by the high-power density laser via the bright spot effect.[27,28] As the femtosecond laser is focused inside the glass sample, the laser pulse energy is nonlinearly absorbed through generating and heating of free electrons, and thus the dense plasma is produced at the center of the molten area. As the electrons in the plasma transfer energy to ions by Coulomb collisions, the hydrodynamic motion of ions start, and the shock wave is generated around the energy deposition zone. This means that the microexplosion occurs and the initial void structures are created in the glass melt.[2] At the border of the plasma area there should be a negative charge due to the difference in average velocity between electrons and ions. The charged surface is naturally characterized by the surface repulsion coefficient which increases with temperature. However, the surface tension coefficient decreases with temperature. The balance between surface repulsion force, surface tension force as well as the gas pressure inside leads to the voids' formation after a single pulse of the femtosecond laser and subsequently merging to small bubbles.[27,28]

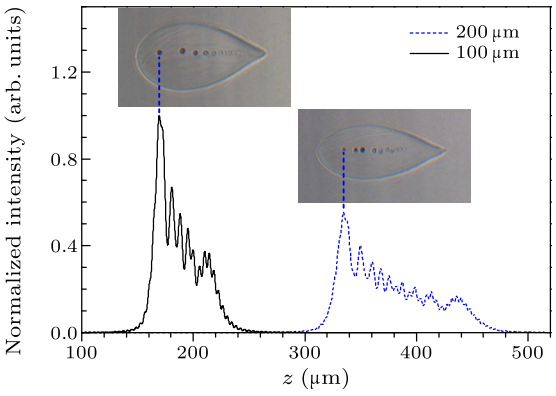

Fig. 3. Calculated results of axial intensity distribution along the laser beam propagation under the focal depths of 100 μm and 200 μm. The inserted images are the cross section of the femtosecond laser irradiated areas with the irradiation time of 1/125 s.

To investigate the formation of bubble patterns, the on-axis laser intensity distribution is simulated via the theory of interface spherical aberration effect,[29,30] which describes the distortions of the light field around the focal region as the laser is focused by a high-aperture lens through an interface with refractive index mismatch. The simulation results along the z-axis under the focal depth of 100 μm and 200 μm are presented in Fig. 3. It is evident that the focused beam intensity distribution spreads along the propagation direction with a single main maximum and several minor maxima, indicating that the quasiperiodic plasma might be generated along the laser beam propagation axis. For a better comparison, the side view image of the focal area under the shortest exposure time is shown by the insets in Fig. 3. It is obvious that the pattern of the bubbles in the cross-section structure is in good agreement with the simulated peaks' distribution along the laser propagation axis, which indicates that the bubbles are induced by quasiperiodic plasma along the laser beam propagation axis simultaneously. However, the axial beam intensity distribution range becomes longer with the increase of the focal depth due to the separation of focal point. Thus the incident laser energy is decentralized for the expansion of exposure range, which makes the beam intensity at focal depth larger than 400 μm too weak to induce bubble structure. Unlike the void structure induced by the single ultrafast laser pulse in transparent solids, the bubbles generated by the high repetition femtosecond laser exist in the glass melt during the irradiation period of time. Thus the motion of the bubbles in the glass melt is affected by several forces. When the glass melt is formed during irradiation, the viscous drag force will affect the moving velocity of the bubbles, and also the buoyancy force moves the bubbles upward in the glass melt.[19,20] Thus we can imagine that thermal gravity convection occurs in the glass melt, and the viscous drag force as well as the buoyancy force makes the bubbles directly move upward and combine to a larger one which is restricted by the boundary of the glass melt. However, at the focal depth of 200 μm, the boundary of the melt area is smaller than that at the focal depth of 100 μm in the same irradiation duration, and the thermal gravity convection may be more turbulent. The small bubbles cannot combine to a large one immediately, and they move around the top area of the melt area driven by viscous drag force of the running glass melt. As the irritation time increases, these small bubbles collide with one another and combine to larger bubbles gradually just as the case at the focal depth of 100 μm. These processes are shown in Fig. 4. The amount of the bubbles below the focal area also grows with the increase of the irradiation time. These bubbles may be driven by the forces from the pressure wave of the microexplosion.[2,19] The existing theory about

temperature distribution around the focal area is developed based on the assumption of constant thermal diffusion coefficient, which means that the heat transfer via thermal convection is ignored.[22] The theory may be improved by taking thermal convection into consideration.

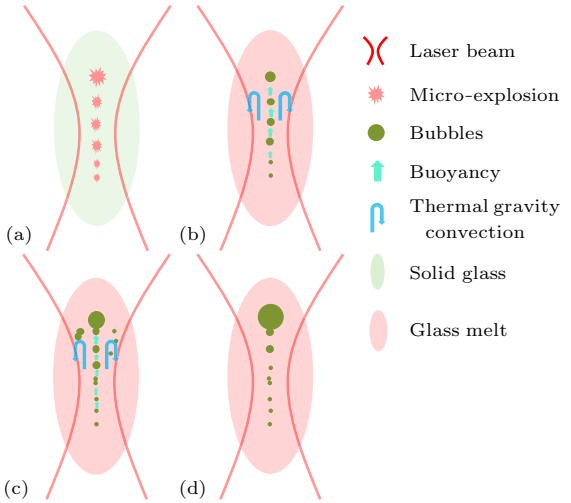

Fig. 4. Schematic diagram of the bubble generation and migration. Micro-explosions are induced by tightly focused femtosecond laser along the laser propagation axis simultaneously in (a). As the irradiation of the laser continues, bubbles are generated in (b). Driven by buoyancy and the viscous drag force of the thermal gravity convection in (c), bubbles move around to merge together. (d) Most of the bubbles are combined into large bubbles at the top of the melting area.

To have a clearer picture of the laser-induced bubbles, we employed a confocal micro Raman mapping to examine the composition of the gas around the bubbles. In the experiment, for better contrast we chose the largest bubble formed under the condition of laser power of 700 mW, focal depth of 100 μm and irradiation time of 8 s. Figures 5(c) and 5(d) show the linear mapping results of the Raman spectra collected along a single line in Figs. 3(a) and 4(b) crossing this bubble. The micro Raman analysis results are shown in Figs. 5(c) and 5(d). The Raman spectra are consistent with the results of previous reports, in which the germanate glass shows three characteristic bands at 538 cm^{-1}, 821 cm^{-1} and 912 cm^{-1}.[23,31] The 538 cm^{-1} band is assigned to symmetric stretching of Ge–O–Ge bonds associated with three-membered ring formation of GeO_4 tetrahedra, and the two high-frequency bands at 821 and 912 cm^{-1} can be ascribed to transverse optic/longitudinal optic (TO/LO) splitting of the antisymmetric stretching of Ge–O–Ge bonds within the network.[32] The intensity distribution of these three bands along the solid line is compared, as shown in Figs. 4(c) and 4(d). Typical Raman signatures due to crystallization cannot be observed. Interestingly, a distinct molecular O_2 peak is identified at 1556 cm^{-1} at locations inside the bubble, as shown in Fig. 5. There are no similar peaks observed outside of the bubble, indicating that the previous signal does not come from the background of atmospheric oxygen.

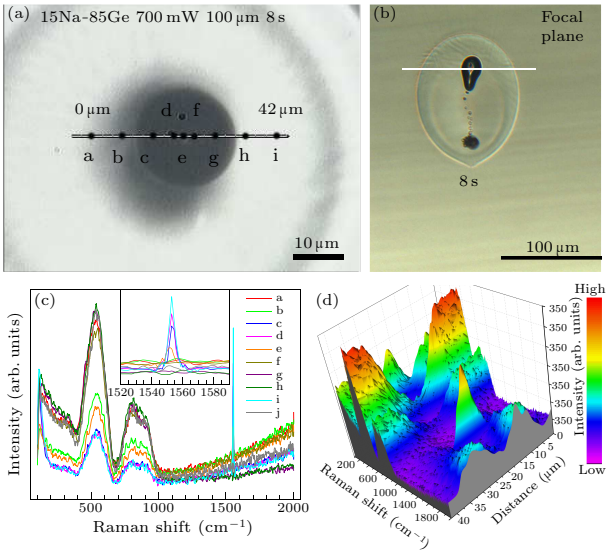

Fig. 5. Optical image and Raman spectra of the femtosecond-laser-irradiated region. (a) Top- and (b) side-view optical transmission images of the bubble in the structure induced by the femtosecond laser with the average power of 700 mW, focal depth of 100 μm and irradiation time of 8 s. (c, d) Line mapping of confocal micro Raman spectra with a step of 2 μm, whose track is shown in (a). The spectra with different colors correspond to the different locations a–i in (a). The micro Raman spectrum of the untreated area is shown as j in (c).

The formation of molecular oxygen from GeO_2 glass has been reported under the conditions of confined micro-explosion where high-p, T zones induced by single, tightly focused, fs-laser pulses might be understood via a scenario similar to that explaining the spatial separation of Al–O ions in sapphire.[3,4] Femtosecond laser pulses with intensity above the optical breakdown threshold break bonds of GeO_2 glass and ionize the constituent atoms into high temperature/density plasma, which is present until the material cools down below the thermal ionization threshold, before the coming of the next pulse. In the presence of this plasma, the diffusion and scattering of Ge and O ions are controlled by the Coulomb collisions, by which the energy transfers from electrons to ions. In that case the heavier Ge ions leave behind the lighter O ions, resulting in the spatial separation of the GeO_2 glass constituents.[2–4] As soon as the temperature of the plasma drops below a certain level, the molecular oxygen might be formed from O ions by releasing the electrons. Based on established theories, these series of processes would finish within a timescale of ∼ps. Nevertheless, the molecular oxygen separated from the glass constituents permanently exists inside the void structures or cracks due to the micro-explosion.[1–3]

In conclusion, we have presented the results of how

experimental parameters affect the morphology of patterned structures as well as bubbles induced by the laser inside the germanate glass by using a 250 kHz repetition rate femtosecond laser. The refractive index changes and the bubble structures around the laser modified region can be clearly observed from optical images. The large bubble structures with oxygen molecules inside are observed by the confocal micro Raman spectra mapping. The molecular oxygen is generated via ion separation inside the plasma induced by ultrashort laser single pulses, which also cause the formation of voids in germanate glass by confined microexplosion. These voids containing oxygen merge into small bubbles, whose motion is affected by viscous drag force and the buoyancy. The thermal gravity convection of the glass melt around focal area is observed, indicating a new way of heat and material transfer in laser–material interaction, which have certain implications for the improvement of the existing thermal diffusion model and the element distribution theory. The present result is important for understanding the origin of bubbles as well as the heat modifications under an ultrafast laser in glass materials, which may have potential applications in fabrication of integrated optical devices, such as waveguides and photonic crystals inside glasses.

References

[1] Juodkazis S, Nishimura K, Tanaka S, Misawa H, Gamaly E G, Luther-Davies B, Hallo L, Nicolai P and Tikhonchuk V T 2006 *Phys. Rev. Lett.* **96** 166101

[2] Gamaly E G, Juodkazis S, Nishimura K, Misawa H and Luther-Davies B 2006 *Phys. Rev.* B **73** 214101

[3] Bressel L, de Ligny D, Gamaly E G, Rode A V and Juodkazis S 2011 *Opt. Mater. Express* **1** 1150

[4] Vailionis A, Gamaly E G, Mizeikis V, Yang W, Rode A V and Juodkazis S 2011 *Nat. Commun.* **2** 445

[5] Itoh K, Watanabe W, Nolte S and Schaffer C B 2006 *MRS Bull.* **31** 620

[6] Miura K, Qiu J R, Fujiwara S, Sakaguchi S and Hirao K 2002 *Appl. Phys. Lett.* **80** 2263

[7] Schaffer C B, Brodeur A, Garcia J F and Mazur E 2001 *Opt. Lett.* **26** 93

[8] Eaton S M, Merchant C A, Iyer R, Zilkie A J, Helmy A S, Aitchison J S, Herman P R, Kraemer D, Miller R, Hnatovsky C and Taylor R S 2008 *Appl. Phys. Lett.* **92** 081105

[9] Liao Y, Song J, Li E, Luo Y, Shen Y, Chen D, Cheng Y, Xu Z, Sugioka K and Midorikawa K 2012 *Lab. Chip.* **12** 746

[10] Dai Y, Zhu B, Qiu J R, Ma H L, Lu B, Cao S X and Yu B K 2007 *Appl. Phys. Lett.* **90** 181109

[11] Watanabe T, Shiozawa M, Tatsu E, Kimura S, Umeda M, Mine T, Shimotsuma Y, Sakakura M, Nakabayashi M, Miura K and Watanabe K 2013 *Jpn. J. Appl. Phys.* **52** 09LA02

[12] Sankin G N, Simmons W N, Zhu S L and Zhong P 2005 *Phys. Rev. Lett.* **95** 034501

[13] Quinto-Su P A, Huang X H, Gonzalez-Avila S R, Wu T and Ohl C D 2010 *Phys. Rev. Lett.* **104** 014501

[14] Uebbing J J, Hengstler S, Schroeder D, Venkatesh S and Haven R 2006 *J. Microelectromech. Syst.* **15** 1528

[15] Glezer E N and Mazur E 1997 *Appl. Phys. Lett.* **71** 882

[16] Bellouard Y and Hongler M O 2011 *Opt. Express* **19** 6807

[17] Graf R, Fernandez A, Dubov M, Brueckner H J, Chichkov B N and Apolonski A 2007 *Appl. Phys.* B **87** 21

[18] Thomas J, Bernard R, Alti K, Dharmadhikari A K, Dharmadhikari J A, Bhatnagar A, Santhosh C and Mathur D 2013 *Opt. Commun.* **304** 29

[19] Luo F F, Lin G, Sun H Y, Zhang G, Liu L, Chen D P, Chen Q X, Zhao Q Z, Qiu J R and Xu Z Z 2011 *Opt. Commun.* **284** 4592

[20] Ye J Y, Chang G, Norris T B, Tse C, Zohdy M J, Hollman K W, O'D M, Baker Jr J R et al 2004 *Opt. Lett.* **29** 2136

[21] Mermillod-Blondin A, Burakov I M, Meshcheryakov Y P, Bulgakova N M, Audouard E, Rosenfeld A, Husakou A, Hertel I V and Stoian R 2008 *Phys. Rev.* B **77** 104205

[22] Shimizu M, Sakakura M, Ohnishi M, Shimotsuma Y, Nakaya T, Miura K and Hirao K 2010 *J. Appl. Phys.* **108** 073533

[23] Liu Y, Shimizu M, Wang X, Zhu B, Sakakura M, Shimotsuma Y, Qiu J R, Miura K and Hirao K 2009 *Chem. Phys. Lett.* **477** 122

[24] Liu Y, Zhu B, Dai Y, Qiao X S, Ye S, Teng Y, Guo Q T, Ma H L, Fan X P and Qiu J R 2009 *Opt. Lett.* **34** 3433

[25] Tu Z F, Teng Y, Zhou J J, Zhou S F, Zeng H P and Qiu J R 2013 *J. Raman Spectrosc.* **44** 307

[26] Sun M Y, Eppelt U, Schulz W G and Zhu J Q 2013 *Opt. Mater. Express* **3** 1716

[27] Yakovlenko S I 2006 *International Conference on Lasers, Applications, and Technologies 2005: Laser-Assisted Micro- and Nano-technologies* **6161** M1610

[28] Yakovlenko S I 2004 *Quantum Electron.* **34** 765

[29] Torok P, Varga P, Laczik Z and Booker G R 1995 *J. Opt. Soc. Am.* A **12** 325

[30] Dai Y, Yu G J, Wu G R, Liang M H, Yan X N and Ma G H 2012 *Chin. Phys.* B **21** 025201

[31] Wang X, Sakakura M, Liu Y, Qiu J, Shimotsuma Y, Hirao K and Miura K 2011 *Chem. Phys. Lett.* **511** 266

[32] Henderson G S and Fleet M E 1991 *J. Non-Cryst. Solids* **134** 259